

Anomalous plasma acceleration in colliding high-power laser-produced plasmas

T. Morita,^{1, a)} K. Nagashima,² M. Edamoto,² K. Tomita,¹ T. Sano,³ Y. Itadani,² R. Kumar,⁴ M. Ota,⁴ S. Egashira,⁴ R. Yamazaki,⁵ S. J. Tanaka,⁵ S. Tomita,⁵ S. Tomiya,⁵ H. Toda,⁵ I. Miyata,⁵ S. Kakuchi,⁵ S. Sei,⁵ N. Ishizaka,⁵ S. Matsukiyo,¹ Y. Kuramitsu,⁶ Y. Ohira,⁷ M. Hoshino,⁷ and Y. Sakawa³

¹⁾*Faculty of Engineering Sciences, Kyushu University, 6-1 Kasuga-Koen, Kasuga, Fukuoka 816-8580,*

Japan

²⁾*Interdisciplinary Graduate School of Engineering Sciences, Kyushu University, 6-1, Kasuga-Koen, Kasuga, Fukuoka 816-8580,*

Japan

³⁾*Institute of Laser Engineering, Osaka University, 2-6 Yamadaoka, Suita, Osaka 565-0871,*

Japan

⁴⁾*Graduate School of Science, Osaka University, 1-1 Machikane-yama, Toyonaka, Osaka 560-0043,*

Japan

⁵⁾*Department of Physics and Mathematics, Aoyama Gakuin University, 5-10-1 Fuchinobe, Sagamihara, Kanagawa 252-5258,*

Japan

⁶⁾*Graduate School of Engineering, Osaka University, 2-1 Yamadaoka, Suita, Osaka 565-0871,*

Japan

⁷⁾*Department of Earth and Planetary Science, University of Tokyo, Bunkyo, Tokyo 113-0033,*

Japan

(Dated: 9 September 2019)

We developed an experimental platform for studying magnetic reconnection in an external magnetic field with simultaneous measurements of plasma imaging, flow velocity, and magnetic-field variation. Here, we investigate the stagnation and acceleration in counter-streaming plasmas generated by high-power laser beams. A plasma flow perpendicular to the initial flow directions is measured with laser Thomson scattering. The flow is, interestingly, accelerated toward the high-density region, which is opposite to the direction of the acceleration by pressure gradients. This acceleration is possibly interpreted by the interaction of two magnetic field loops initially generated by Biermann battery effect, resulting in a magnetic reconnection forming a single field loop and additional acceleration by a magnetic tension force.

Magnetic fields in plasmas have significant roles in thermalization, acceleration, and hydrodynamic turbulence in wide range of plasma parameters, for example, from low- β to high- β conditions, where β is the ratio of thermal to magnetic pressures. Magnetic reconnection (MR) is the most important mechanism in the global change of magnetic field topology and rapid energy transfer from the field to particles in fusion plasmas, magnetic storms in the earth's magnetosphere, solar eruptions, and magnetic fields in most astrophysical contexts¹. MR physics can be interpreted as a combination of microscopic dissipation and macroscopic advection in surrounding magnetized plasmas. Previous numerical studies (e.g. magnetohydrodynamic² and full particle-in-cell³ simulations) and observations (including electron and ion velocity distributions measured by the Geotail spacecraft⁴) have approached these two mechanisms from separate viewpoints and this makes it difficult to investigate the physical mechanisms by which energy changes from across large spatial scales, and how the reconnection rate is determined.

Laboratory experiments have an advantage in that various plasma diagnostics can be used simultaneously both for microscopic and macroscopic phenomena. Local plasma parameters and magnetic fields have been precisely diagnosed in gas-discharged plasmas such as TS-3^{5,6}, MRX^{7,8}, and pulse-powered devices^{9,10}, with relatively low-beta ($\beta < 1$).

Recently, strongly-driven MR has been studied using laser-produced plasmas^{11–19} under strong magnetic fields generated by the interaction of high-power lasers with solids via the Biermann battery effect ($\partial B/\partial t \propto \nabla T_e \times \nabla n_e$)²⁰. In contrast to other laboratory experiments, laser-produced plasmas with high temperatures and densities enable us to investigate MR in high-beta conditions, similar to those in magnetosheath ($\beta \sim 0.1–10$)²¹ and in accretion disks ($\beta > 10$)²². However, few diagnostics are available in such small-scale plasmas, and recent studies have focused on topological change in a field^{13–15}, global plasma structure^{17–19}, and numerical simulations^{11,12}. Although spatially and temporally resolved measurements of flow velocities, plasma parameters, and magnetic fields are required to fully understand physical processes such as the MR rate, no direct measurement of plasma parameters in inflow or outflow and magnetic fields have been performed in laser-plasma experiment.

We implemented an experimental system for studying the MR with simultaneous measurements of plasma imaging, flow velocity, and magnetic-field variation in an external magnetic field. In this letter, we investigate counter-streaming plasma interactions, stagnation, and acceleration perpendicular to the initial flow directions. The plasma is, interestingly, accelerated toward higher-pressure region, showing strong temporal and spatial dependence. This anomalous flow is possibly interpreted as the acceleration by a magnetic tension force from a distorted magnetic field, resulting from the MR between anti-parallel fields initially generated via Biermann battery effects and advected with expanding plasma²³.

^{a)}Electronic mail: morita@ees.kyushu-u.ac.jp.

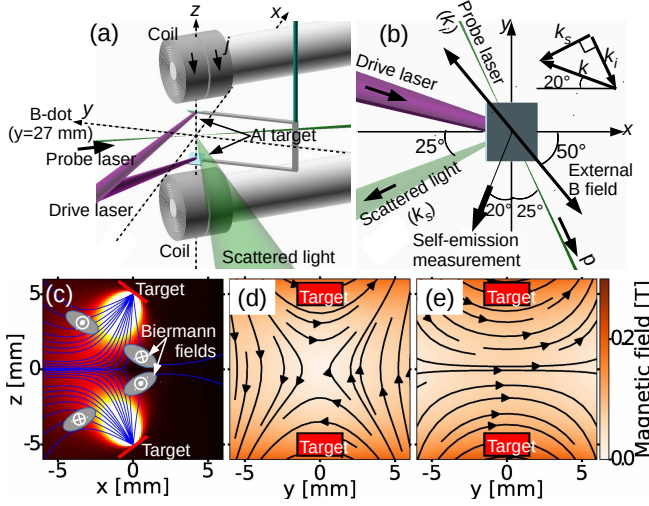


FIG. 1. (a) Schematic of the experimental setup with two electro-magnetic coils and two targets. The drive laser and probe laser for TS measurement are also shown. (b) The top view of the setup. The probe laser (k_i) and the direction of the scattered light (k_s) determine the k -vector. (c) Calculated electron streams from tilted targets, as well as the Biermann field in the x - z plane. The external magnetic fields are generated by driving two coils in the y - z plane, (d) in opposite directions (anti-parallel) and (e) in the same direction (parallel).

The experiment was conducted with Gekko-XII laser beams at the Institute of Laser Engineering, Osaka University. Figure 1(a) shows the schematic of the experimental setup. Two laser beams (drive laser: output energy 600 J in a 1.3 ns Gaussian pulse with wavelength 1053 nm) irradiate two aluminum foils (with thickness 200 μm and separation 10 mm) with focal spot diameters of $\sim 300 \mu\text{m}$, to produce two plasma flows between them. The targets are tilted 30° from the horizontal plane to produce tilted flows in the x - z plane as shown in Fig. 1(c). Plasma flow velocity was measured with laser Thomson scattering (TS) in the center of the targets. A probe laser (Nd:YAG laser, wavelength 532 nm, energy 370 mJ in 10 ns, wavenumber vector k_i) penetrated the plasma in the horizontal plane ($z = 0$) at an angle of 65° from the x -axis, and the scattered light (k_s) was collected 90° from the incident direction, forming the measurement wavenumber, $k = k_s - k_i$ as shown in Fig. 1(b) (20° rotated from the x -axis). The scattered light was guided to a high-resolution ($\sim 14 \text{ pm}$) spectrometer with triple gratings²⁴ and recorded with an intensified charge-coupled device (ICCD) with an exposure time of 5 ns. The expanding plasmas were imaged with a framing camera at the wavelength of 450 nm with an interference filter with the bandwidth of 10 nm (FWHM). In addition, a magnetic-field variation (ΔB_z) at $y = 27 \text{ mm}$ was measured with a B-dot probe consisting of two inversely directed loops. Most of the electromagnetic noise is reduced by taking difference between the voltages from these loops.

As studied in many experiments with laser-produced counter-streaming plasmas^{25–33}, the magnetic field originated around the laser spot (by the Biermann battery effect) is frozen into the ablation plasma and is advected along electron stream

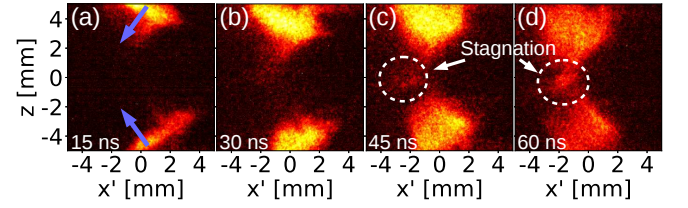


FIG. 2. Self-emission from laser-produced plasmas at the wavelength of 450 nm at $t =$ (a) 15 ns, (b) 30 ns, (c) 45 ns, and (d) 60 ns, taken with a framing camera.

lines²³ because of the large magnetic Reynolds number. Note that the typical time scale of the Bierman battery effect τ_{Bir} is comparable to the laser pulse duration $\sim 1 \text{ ns}$, which is much smaller than typical time scale of plasma dynamics $\tau_{\text{dyn}} \sim 40 \text{ ns}$ in the present study. The electron stream lines are estimated and plotted for tilted targets [Fig. 1(c)]. Here, the electron flux is evaluated as $\phi(r, \theta) \propto \exp[-K(1 - \cos \theta)]/r^2$, where r and θ represent the distance from the laser spot and the angle from the normal direction, respectively, and K characterizes the divergence as discussed in Ref. 23. When the targets are parallel²³, the toroidal magnetic fields from the top and bottom targets encounter each other in the mid-plane. On the other hand, the toroidal fields interact only around the mid-point in the tilted flows as shown in Fig. 1(c).

In addition, an external magnetic field was applied with two 20-turn coils located at $z = \pm 17 \text{ mm}$ along the axis at 40° from the y -axis, as shown with an arrow in Fig. 1(b). They are driven separately by a pulse-powered device³⁴. An anti-parallel [Fig. 1(d)] field enhances the y -component of the Biermann fields ($B_{\text{Bir},y}$) both for $z > 0$ and $z < 0$, while a parallel [Fig. 1(e)] field weakens $B_{\text{Bir},y}$ for $z < 0$. In the present experiment, a magnetic field strength of 0.1 T at the target positions was achieved by applying 200 V on a 6-mF capacitor³⁵ for each coil, producing a more or less constant field during $\sim 100 \mu\text{s}$.

Figure 2 shows the time-evolution of the plasma after the laser irradiation on two aluminum foils measured at 20° from the y -axis, as shown in Fig. 1(b) (the horizontal axis x' is the axis 20° rotated from x) with the anti-parallel external field [Fig. 1(d)]. Note that the external field does not affect the initial super-Alfvénic flows. These are flows for which the Alfvén Mach number $M_A = v/v_A \gtrsim 51$, and hence the magnetic pressure P_M is much smaller than the ram pressure ρv^2 ($P_M/\rho v^2 = 1/2M_A^2 \lesssim 2 \times 10^{-4}$), where $v \gtrsim 125 \text{ km/s}$ is the flow velocity estimated at $t < 40 \text{ ns}$, $v_A = 2.5 \pm 0.4 \text{ km/s}$ is the Alfvén velocity in an external magnetic field of 0.1 T [two different geometries are shown in Figs. 1(d) and 1(e)] with ion density $n_i = (2.9 \pm 0.5) \times 10^{22} \text{ m}^{-3}$ estimated from TS spectrum at $t = 40 \text{ ns}$; this will be discussed later in Fig. 3(f). As the plasmas expand from top and bottom, two flows interact to form a dense plasma which is observed in the mid-plane at $t \gtrsim 45 \text{ ns}$. Note that this dense plasma is reproducibly observed in different laser shots (not shown) at $-4 \text{ mm} < x' < -1 \text{ mm}$.

Figures 3(b)–3(d) show the TS spectra at $t = 30, 40,$

and 50 ns, respectively, with the anti-parallel external magnetic field [Fig. 1(d)]. The vertical axis shows the position along the probe laser [p -axis: $(x, y) = (p \cos 65^\circ, p \sin 65^\circ)$] and the horizontal axis represents the wavelength difference $\Delta\lambda = \lambda - \lambda_0$, where λ_0 is the incident laser wavelength. A bright stray light is observed at $\Delta\lambda = 0$. As illustrated in Fig. 1(a), the plasma parameters parallel to k are obtained in this measurement. Figures 3(e)–3(g) show the line-out plots for $p = 0$ mm at $t = 30, 40,$ and 50 ns, respectively. Two peaks of the ion acoustic resonance are seen in Fig. 3(f), where one of them overlaps with the stray light (the shaded area). The solid lines in Figs. 3(f) and 3(g) show the best-fit results with a theoretical function³⁶ convoluted with the spectral resolution³⁷ (estimated from Rayleigh scattering), where the charge state Z is self-consistently obtained from a collisional radiative model with FLYCHK code³⁸. Note that this model is valid, in general, in highly ionized and moderate density plasmas, as observed in the present experiment, between high-density (local thermal equilibrium) and low-density (coronal equilibrium) limits, where excited populations are determined by collisional and radiative processes. At $t = 40$ ns, the fitting gives electron and ion temperatures of $T_e = 92 \pm 35$ eV and $T_i = 75 \pm 14$ eV, respectively, electron density $n_e = (2.6 \pm 0.4) \times 10^{23} \text{ m}^{-3}$, and average charge state $Z = 9.0 \pm 1.0$. At $t = 50$ ns, the corresponding values are $T_e = 74 \pm 23$ eV, $T_i = 87 \pm 17$ eV, $n_e = (1.6 \pm 0.2) \times 10^{23} \text{ m}^{-3}$, and $Z = 8.1 \pm 0.8$. In general, ion-feature is in collective regime when $\alpha \gtrsim (ZT_e/3T_i - 1)^{-1/2}$ ³⁶, where $\alpha = 1/k\lambda_D$ and λ_D is the Debye length. Although the ion-acoustic wave is weakly damped at $t = 40$ ns ($\alpha = 0.43 \pm 0.09$ is slightly under $(ZT_e/3T_i - 1)^{-1/2} = 0.62 \pm 0.19$), the ion-acoustic resonance is clearly seen for $-4 \text{ mm} < p < 2 \text{ mm}$ in Fig. 3(c), and $-4 \text{ mm} < p < 0 \text{ mm}$ in Fig. 3(d). On the other hand, no ion-acoustic resonance is observed at $t = 30$ ns [Fig. 3(e)]. Assuming the non-collective ion-feature of the ion thermal distribution as Maxwellian, a large ion temperature of $T_i = 1.2 \pm 0.1$ keV is obtained as shown by the solid line in Fig. 3(e), indicating small ZT_e/T_i and strong damping of ion-acoustic waves.

The flow velocity along k (v_k) can be estimated from the deviation of the spectrum from $\Delta\lambda = 0$ (Doppler effect) in both the collective and non-collective regimes. The standard errors are estimated by non-linear least square fitting and are smaller than the marks in most of data points in Figs. 3(h)–3(j). Although there are systematic errors, namely the pointing of the probe laser (< 0.1 mm) and timing jitter of the detector (~ 35 ps), both are ignorable when determining v_k . Early and late in time, as shown in Figs. 3(b) and 3(e) ($t = 30$ ns), and 3(d) and 3(g) ($t = 50$ ns), respectively, the flow velocity is small for $p \sim 0$ mm ($v_k = 4.1 \pm 1.4$ km/s and 2.8 ± 0.9 km/s from Figs. 3(e) and 3(g), respectively). In contrast, the TS spectrum obtained at $t = 40$ ns [Figs. 3(c) and 3(f)], is blue-shifted at $p < 2$ mm which means that the plasma flows into the positive k -direction ($v_k = 40 \pm 3$ km/s at $p = 0$). This tendency is seen in Fig. 3(h), where v_k is plotted as a function of p measured at $t = 30, 40, 50,$ and 80 ns.

As illustrated in Fig. 3(a), the plasma flow in the case of free streaming can be estimated as $v_{k,\text{free}} = -v_{\text{flow}} \sin \theta \cos 45^\circ$, where $v_{\text{flow}} = (L^2 + p^2)^{1/2}/t$ is the flow

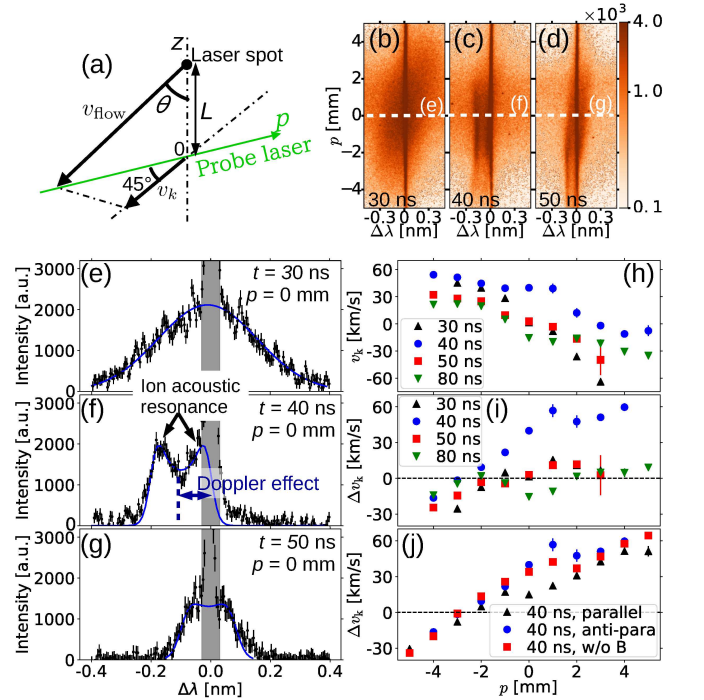


FIG. 3. (a) The relation between the flow velocity from the upper target (v_{flow}) and the measured velocity (v_k). TS spectra are given at (b) 30 ns, (c) 40 ns, and (d) 50 ns along the probe laser axis. The origin $p = 0$ corresponds to the midpoint between two laser spots. The line-out plots are given at (e) 30 ns, (f) 40 ns, and (g) 50 ns for $p = 0$ mm. The solid lines show the best-fit results. (h) shows v_k and (i) shows the velocity difference Δv_k measured for different delay times with an anti-parallel external field, and (j) shows Δv_k in different external field configurations.

velocity from the laser spot to the measured position, θ is the angle defined in Fig. 3(a), L is the half distance between two laser spots, and t is the time from the drive laser timing. $v_{k,\text{free}}$ is a good estimation for the flow velocity even in counter-streaming plasmas as observed in similar experimental configurations in Refs. 28 and 37, in which slow-down of each flow is only 10–20%. Figure 3(i) shows the difference between the measured velocity v_k and the calculated velocity $v_{k,\text{free}}$, $\Delta v_k = v_k - v_{k,\text{free}}$. Early and late in time at $t = 30, 50,$ and 80 ns, although $\Delta v_k \sim 0$ near the center $p \sim 0$, $|v_k| < |v_{k,\text{free}}|$ far from the center due to the slow-down of the plasma flow. Note that the slow-down effect shows $\Delta v_k > 0$ and $\Delta v_k < 0$ for $p > 0$ and $p < 0$, respectively. While this slow-down effect on Δv_k is less than 30 km/s, the velocity difference of ~ 60 km/s at $t = 40$ ns is much larger than that at $p \sim 1$ mm, meaning that another acceleration occurs only at this time. Figure 3(j) shows Δv_k under three different external field conditions: with an anti-parallel field [Fig. 1(d)], with a parallel field [Fig. 1(e)], and without the external field. The measured velocity with an anti-parallel field ($\Delta v_k = 57 \pm 5$ km/s) is larger than that without the external field ($\Delta v_k = 42 \pm 1$ km/s) at $p = 1$ mm. All TS data with different times and external field conditions are taken in different laser shots, indicating that the

acceleration along k at $t = 40$ ns is reproducible as expressed in Fig. 3(j).

Two possibilities may explain this anomalous acceleration: (1) a pressure increase in the mid-plane resulting from the collision of two plasma flows, and (2) MR between toroidal fields generated via the Biermann battery effect. For the former case, assuming 100% energy conversion from initial kinetic energy to thermal energy in the mid-plane, and the resultant kinetic energy accelerated by the thermal pressure, a value of $v_k < 125$ km/s (estimated with $L = 5$ mm and $t = 40$ ns) can be explained. It might be possible that the hydrodynamic jet is driven from the stagnation point where two plasmas collide with each other forming higher pressure at $x \sim -2$ mm as shown in Figs. 2(c) and 2(d). This flow (along pressure gradients) has negative Δv_k at $x \sim 0$, while we observe the positive Δv_k as shown in Figs. 3(i) and 3(j). This indicates that the observed flow in the k -direction [see Figs. 3(i) and 3(j)] is not explained by the pure hydrodynamics, but is rather interpreted as the acceleration by the magnetic field. In this case, the Biermann fields become flat structures as they collide with each other and stagnate in the mid-plane as demonstrated in Ref. 39 even in a tilted geometry similar to the present experiment. These fields [Fig. 4(a)] can reconnect with each other as illustrated in Fig. 4(b), forming a bent loop as shown in Ref. 40. The thickness of the magnetic diffusion region for the MR is comparable to the ion inertial length¹, $\delta_z \sim c/\omega_{pi} = 0.77 \pm 0.16$ mm, calculated with the parameters obtained from the TS spectrum at $t = 40$ ns [Fig. 3(f)]. This small MR region indicates quasi-two-dimensional MR in the y - z plane because B_x is small ($B_{\text{Bir},x}/B_{\text{Bir},y} \sim \delta_x/\delta_y \sim 0.29$, where $\delta_x \sim \delta_z$ and $\delta_y \sim [R^2 - (R - \delta_x)^2]^{1/2} \sim 2.7$ mm are the lengths of the diffusion region in the x and y -directions assuming a large curvature radius of the Biermann field $R = L = 5$ mm), and the MR should initially produce outflows predominantly in the $\pm y$ -directions as shown in Fig. 4(c).

Here, the magnetic Reynolds number in the present experiment is large: $R_M = Lv/D_M = (2.2 \pm 1.1) \times 10^2$, where $L \sim 5$ mm is the scale length, $v \sim 125$ km/s at $t = 40$ ns is the vertical flow velocity, $D_M = v_{ei}(c/\omega_{pe})^2 = 2.8 \pm 1.4$ m²/s is the magnetic diffusivity, $v_{ei} = (2.6 \pm 1.4) \times 10^{10}$ s⁻¹ is the electron-ion collision frequency⁴¹, and $c/\omega_{pe} = 10 \pm 2$ μ m is the electron skin depth. Typically, ideal magnetohydrodynamics (MHD) can be applied⁴² to plasmas with R_M larger than 10. In addition, larger R_M ($\sim 10^2$ – 10^3) enables us to investigate MR with a current sheath much thinner than typical plasma scale⁴². The magnetic force acting on the unit volume of the plasma is expressed as

$$\begin{aligned} f &= j \times B = (\nabla \times B) \times B / \mu_0 \\ &= -\nabla(B^2/2\mu_0) + B \cdot \nabla B / \mu_0 \\ &= -\nabla_{\perp}(B^2/2\mu_0) - B^2 \hat{r}_c / \mu_0 r_c = f_p + f_t, \end{aligned}$$

where μ_0 is the vacuum permeability; ∇_{\parallel} and ∇_{\perp} are the gradients parallel and perpendicular to the magnetic field, respectively; and r_c and \hat{r}_c are the curvature radius and the unit vector along the radial direction, respectively. The first term f_p represents the magnetic pressure gradient force perpendicular to the field line, and the second term f_t expresses the mag-

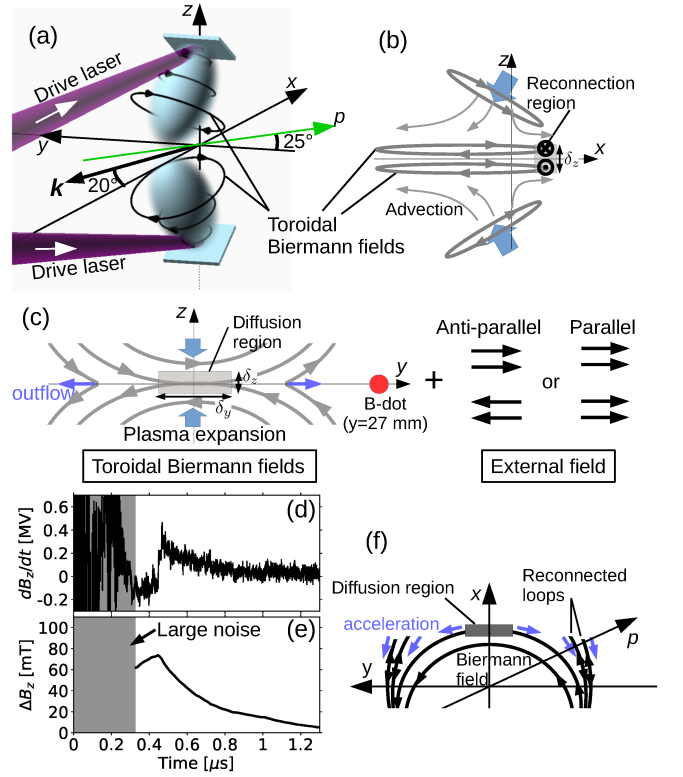


FIG. 4. (a) Three-dimensional and (b) two-dimensional (in the x - z plane) cartoons of the toroidal Biermann fields in the top and bottom plasmas. (c) Two toroidal fields interact in the mid-plane as shown in a two-dimensional view (in the y - z plane) with two different configurations of external magnetic fields. (d) Time-derivative of the magnetic-field variation (dB_z/dt) and (e) the calculated magnetic-field deviation ΔB_z from the constant field later in time ($t > 2$ μ s) measured at $y = 27$ mm. (f) The schematic view of the field lines in the x - y plane after MR.

netic tension force when the field line curves. While f_p acts isotropically vertical to the field, f_t accelerates the plasma towards \hat{r}_c . This tension force acts in the $\pm y$ -direction near the diffusion region generating an outflow from MR, which is quasi-two-dimensional [see the left figure in Fig. 4(c)]. The plasma is accelerated on a typical scale of l in the acceleration time of $\Delta t \sim (2l/a)^{1/2}$ where $a = f_t/m_i n_i$ is the acceleration. The resultant plasma velocity becomes

$$\begin{aligned} v_{\text{acc}} &\sim |a|\Delta t = (2la)^{1/2} = B(2/\mu_0 m_i n_i)^{1/2} (l/r_c)^{1/2} \\ &\sim B(2/\mu_0 m_i n_i)^{1/2} \sim v_A, \end{aligned} \quad (1)$$

where $n_i = (2.9 \pm 0.5) \times 10^{22}$ m⁻³, and the acceleration distance l is comparable to the curvature radius $l \sim r_c$. The time-derivative of the magnetic-field variation in the z -component (dB_z/dt) and the magnetic-field deviation [$\Delta B_z = -\int_{2\mu\text{s}}^t (dB_z/d\tau) d\tau$] from a constant field strength later in time (> 2 μ s), without the external magnetic field, are shown in Figs. 4(d) and 4(e), respectively. Although the magnetic field early in time is difficult to infer due to large electro-

magnetic noise, a positive ΔB_z is detected at $t \sim 450$ ns, suggesting a magnetized plasma flow with the velocity of ~ 66 km/s [= 27 mm/(450 – 40) ns] assuming MR at $t = 40$ ns, which is comparable to the Alfvén velocity with $B \sim 2.7$ T and $n_i = 2.9 \times 10^{22} \text{ m}^{-3}$ at the acceleration site.

As the reconnected loop expands in $\pm y$, f_t also accelerates the plasma in the $-x$ -direction because the \hat{r}_c of a reconnected field loop is in the $-x$ -direction as shown in the x - z plane [Fig. 4(f)] at $p > 0$. The measured velocity $v_k \sim 57$ km/s can be explained with the field strength of ~ 2.3 T which is slightly smaller than the strength of ~ 2.7 T estimated from the velocity in the y -direction. The initial curvature radius r_c (y -direction) is formed as a result of MR, and the curvature in the x -direction would be comparable to or slightly larger than that as the field expand in the $\pm y$ -directions; $r_c \gtrsim \delta_z \sim c/\omega_{pi} \sim 0.77$ mm. Note that the long diffusion time τ_M of the magnetic field in the typical plasma size of L ($\tau_M = L^2/D_M = (L/v)R_M \sim \tau_{dyn}R_M = 8.8 \pm 4.4 \mu\text{s} \gg \tau_{dyn} \sim 40$ ns for $L = 5$ mm) indicates that only the surface of the expanding plasma is magnetized, and MR occurs only when the plasmas collide with each other at $t \sim 40$ ns. The acceleration due to the magnetic tension force acts on the plasma after the MR, and this is why the TS measures the velocity increase only at $t = 40$ ns.

From Eq. (1), the increment in the velocity from 42 km/s (only the Biermann fields) to 57 km/s (now with the anti-parallel external field) can be explained by a $57/42 \sim 1.4$ times stronger magnetic field, or increment in the field from 1.6 to 2.3 T. Even though the initial external field strength of 0.1 T is weak ($M_A > 52$ at $t < 40$ ns) and does not affect the initial plasma streams, it can be piled up as the plasma expands because of high conductivity, which has already been seen in previous experimental studies^{13,14,16,43,44} by a factor of four, meaning that both parallel and anti-parallel external fields become comparable to the Biermann fields in the interaction region. As investigated in Ref. 23 considering the electron stream, the Biermann field of ~ 50 T (measured in Ref. 45 with a comparable laser intensity) decreases to ~ 4 T as it is advected to 5 mm^{23} , and the reconnected field is even weaker; this agrees well with our estimation of ~ 2.7 T for the acceleration in the y -direction and ~ 1.6 – 2.3 T in the x -direction after MR with and without anti-parallel external magnetic field.

Another possible interpretation for the external magnetic field dependence comes from the x -component of the external magnetic field. The anti-parallel external field ($\pm B_{\text{ext},x}$, $\pm B_{\text{ext},y}$) and the Biermann field (0 , $\pm B_{\text{Bir},y}$) make another anti-parallel field of ($\pm B_{\text{ext},x}$, $\pm B_{\text{ext},y} \pm B_{\text{Bir},y}$) on a different plane rotated around z , where positive and negative signs show the magnetic field in $z > 0$ and $z < 0$, respectively. On the other hand, the parallel external field produces the composite field of ($B_{\text{ext},x}$, $B_{\text{ext},y} \pm B_{\text{Bir},y}$), meaning that the asymmetric MR between $B_{\text{ext},y} \pm B_{\text{Bir},y}$ [see Fig. 4(c)] occurs in a guide field of $B_{\text{ext},x}$. This asymmetric MR decreases the velocity in the mid-plane, resulting in the slowest velocity ($\Delta v_k = 22 \pm 1$ km/s).

In summary, we have investigated the interaction between laser-produced counter-streaming plasmas, stagnation, and acceleration, with newly implemented experimental platform

with self-emission imaging, laser Thomson scattering, and a B-dot probe. The plasma acceleration perpendicular to the initial flow directions is detected. This flow is, interestingly, opposite to the acceleration due to pressure gradients, suggesting other acceleration mechanism. Here, we proposed the acceleration via magnetic tension force in a bent field loop resulting from a MR between two field loops initially generated by a Biermann battery effect and advected with expanding plasmas. Even though further investigation and comparison would be required, the flow velocity changes depending on the external magnetic field direction, indicating that the external field changes the strength and structure of the reconnection field. Interestingly, the acceleration quasi-perpendicular to the y - z plane indicates that the global field structure affects the microscopic plasma flow despite the MR occurring in the quasi-two-dimensional plane. Though there have been no direct observation of this anomalous acceleration, it could be detected, for example, in the turbulent magnetosheath or solar coronal loops, with future high-resolution measurements. Further experimental investigations combining multi-dimensional velocity measurements with local magnetic field measurements will promote greater understanding of not only the physical process but also the plasma dynamics of the MR.

The authors would like to acknowledge the dedicated technical support of the staff at the Gekko-XII facility for the laser operation, target fabrication, and plasma diagnostics. We would also like to thank K. Shibata, N. Yamamoto, A. Asai, and S. Zenitani for helpful comments and valuable discussions. This research was partially supported by JSPS KAKENHI grant numbers 18H01232, 17H06202, 15H02154, 17K14876, and 17H18270, and by the joint research project of Institute of Laser Engineering, Osaka University.

- ¹E. G. Zweibel and M. Yamada, Annual Review of Astronomy and Astrophysics **47**, 291 (2009).
- ²T. Tanaka, A. Nakamizo, A. Yoshikawa, S. Fujita, H. Shinagawa, H. Shimazu, T. Kikuchi, and K. K. Hashimoto, Journal of Geophysical Research: Space Physics **115**, A05220 (2010).
- ³W. Daughton, V. Roytershteyn, H. Karimabadi, L. Yin, B. J. Albright, B. Bergen, and K. J. Bowers, Nature Physics **7**, 539 (2011).
- ⁴T. Nagai, I. Shinohara, M. Fujimoto, A. Matsuoka, Y. Saito, and T. Mukai, Journal of Geophysical Research: Space Physics **116**, A04222 (2011).
- ⁵Y. Ono, A. Morita, M. Katsurai, and M. Yamada, Physics of Fluids B **5**, 3691 (1993).
- ⁶Y. Ono, Y. Hayashi, T. Ii, H. Tanabe, S. Ito, A. Kuwahata, T. Ito, Y. Kamino, T. Yamada, and M. Inomoto, Physics of Plasmas **18** (2011).
- ⁷M. Yamada, H. Ji, S. Hsu, T. Carter, R. Kulsrud, N. Bretz, F. Jobs, Y. Ono, and F. Perkins, Physics of Plasmas **4**, 1936 (1997).
- ⁸Y. Ren, M. Yamada, S. Gerhardt, H. Ji, R. Kulsrud, and A. Kuritsyn, Physical Review Letters **95**, 055003 (2005).
- ⁹J. D. Hare, L. G. Suttle, S. V. Lebedev, N. F. Loureiro, A. Ciardi, J. P. Chittenden, T. Clayson, S. J. Eardley, C. Garcia, J. W. Halliday, T. Robinson, R. A. Smith, N. Stuart, F. Suzuki-Vidal, and E. R. Tubman, Physics of Plasmas **25** (2018).
- ¹⁰J. D. Hare, L. Suttle, S. V. Lebedev, N. F. Loureiro, A. Ciardi, G. C. Burdiak, J. P. Chittenden, T. Clayson, C. Garcia, N. Niasse, T. Robinson, R. A. Smith, N. Stuart, F. Suzuki-Vidal, G. F. Swadling, J. Ma, J. Wu, and Q. Yang, Physical Review Letters **118**, 085001 (2017).
- ¹¹S. R. Titorica, T. Abel, and F. Fiuza, Physics of Plasmas **24** (2017).
- ¹²S. R. Titorica, T. Abel, and F. Fiuza, Physical Review Letters **116**, 095003 (2016).
- ¹³M. J. Rosenberg, C. K. Li, W. Fox, I. Igumenshchev, F. H. Séguin, R. P. Town, J. A. Frenje, C. Stoeckl, V. Glebov, and R. D. Petrasso, Physics of Plasmas **22**, 042703 (2015).
- ¹⁴M. J. Rosenberg, C. K. Li, W. Fox, A. B. Zylstra,

- C. Stoeckl, F. H. Séguin, J. A. Frenje, and R. D. Petrasso, *Physical Review Letters* **114**, 205004 (2015).
- ¹⁵P. M. Nilson, L. Willingale, M. C. Kaluza, C. Kamperidis, S. Minardi, M. S. Wei, P. Fernandes, M. Notley, S. Bandyopadhyay, M. Sherlock, R. J. Kingham, M. Tatarakis, Z. Najmudin, W. Rozmus, R. G. Evans, M. G. Haines, A. E. Dangor, and K. Krushelnick, *Physical Review Letters* **97**, 255001 (2006).
- ¹⁶W. Fox, A. Bhattacharjee, and K. Germaschewski, *Physics of Plasmas* **19**, 056309 (2012).
- ¹⁷Q. L. Dong, S. J. Wang, Q. M. Lu, C. Huang, D. W. Yuan, X. Liu, X. X. Lin, Y. T. Li, H. G. Wei, J. Y. Zhong, J. R. Shi, S. E. Jiang, Y. K. Ding, B. B. Jiang, K. Du, X. T. He, M. Y. Yu, C. S. Liu, S. Wang, Y. J. Tang, J. Q. Zhu, G. Zhao, Z. M. Sheng, and J. Zhang, *Physical Review Letters* **108**, 215001 (2012).
- ¹⁸J. Zhong, Y. Li, X. Wang, J. Wang, Q. Dong, C. Xiao, S. Wang, X. Liu, L. Zhang, L. An, F. Wang, J. Zhu, Y. Gu, X. He, G. Zhao, and J. Zhang, *Nature Physics* **6**, 984 (2010).
- ¹⁹P. M. Nilson, L. Willingale, M. C. Kaluza, C. Kamperidis, S. Minardi, M. S. Wei, P. Fernandes, M. Notley, S. Bandyopadhyay, M. Sherlock, R. J. Kingham, M. Tatarakis, Z. Najmudin, W. Rozmus, R. G. Evans, M. G. Haines, A. E. Dangor, and K. Krushelnick, *Physics of Plasmas* **15**, 092701 (2008).
- ²⁰J. A. Stamper, K. Papadopoulos, R. N. Sudan, S. O. Dean, E. A. McLean, and J. M. Dawson, *Physical Review Letters* **26**, 1012 (1971).
- ²¹L. Trenchi, M. F. Marcucci, G. Pallochchia, G. Consolini, M. B. Bavassano Cattaneo, A. M. Di Lellis, H. Rème, L. Kistler, C. M. Carr, and J. B. Cao, *Journal of Geophysical Research: Space Physics* **113**, A07S10 (2008).
- ²²S. A. Balbus and J. F. Hawley, *Reviews of Modern Physics* **70**, 1 (1998).
- ²³D. D. Ryutov, N. L. Kugland, M. C. Levy, C. Plechaty, J. S. Ross, and H. S. Park, *Physics of Plasmas* **20**, 032703 (2013).
- ²⁴K. Tomita, Y. Sato, S. Tsukiyama, T. Eguchi, K. Uchino, K. Kouge, H. Tomuro, T. Yanagida, Y. Wada, M. Kunishima, G. Soumagne, T. Kodama, H. Mizoguchi, A. Sunahara, and K. Nishihara, *Scientific Reports* **7**, 12328 (2017).
- ²⁵C. M. Huntington, F. Fiuza, J. S. Ross, A. B. Zylstra, R. P. Drake, D. H. Froula, G. Gregori, N. L. Kugland, C. C. Kuranz, M. C. Levy, C. K. Li, J. Meinecke, T. Morita, R. Petrasso, C. Plechaty, B. A. Remington, D. D. Ryutov, Y. Sakawa, A. Spitkovsky, H. Takabe, and H. S. Park, *Nature Physics* **11**, 173 (2015).
- ²⁶Y. Sakawa, T. Morita, Y. Kuramitsu, and H. Takabe, *Advances in Physics: X* **1**, 425 (2016).
- ²⁷W. Fox, G. Fiksel, A. Bhattacharjee, P. Y. Chang, K. Germaschewski, S. X. Hu, and P. M. Nilson, *Physical Review Letters* **111**, 225002 (2013).
- ²⁸J. S. Ross, S. H. Glenzer, P. Amendt, R. Berger, L. Divol, N. L. Kugland, O. L. Landen, C. Plechaty, B. Remington, D. Ryutov, W. Rozmus, D. H. Froula, G. Fiksel, C. Sorce, Y. Kuramitsu, T. Morita, Y. Sakawa, H. Takabe, R. P. Drake, M. Grosskopf, C. Kuranz, G. Gregori, J. Meinecke, C. D. Murphy, M. Koenig, A. Pelka, A. Ravasio, T. Vinci, E. Liang, R. Presura, A. Spitkovsky, F. Miniati, and H. S. Park, *Physics of Plasmas* **19**, 056501 (2012).
- ²⁹D. W. Yuan, Y. T. Li, X. Liu, Y. Zhang, J. Y. Zhong, W. D. Zheng, Q. L. Dong, M. Chen, Y. Sakawa, T. Morita, Y. Kuramitsu, T. N. Kato, H. Takabe, Y. J. Rhee, J. Q. Zhu, G. Zhao, and J. Zhang, *High Energy Density Physics* **9**, 239 (2013).
- ³⁰N. L. Kugland, D. D. Ryutov, P. Y. Chang, R. P. Drake, G. Fiksel, D. H. Froula, S. H. Glenzer, G. Gregori, M. Grosskopf, M. Koenig, Y. Kuramitsu, C. Kuranz, M. C. Levy, E. Liang, J. Meinecke, F. Miniati, T. Morita, A. Pelka, C. Plechaty, R. Presura, A. Ravasio, B. A. Remington, B. Reville, J. S. Ross, Y. Sakawa, A. Spitkovsky, H. Takabe, and H. S. Park, *Nature Physics* **8**, 809 (2012).
- ³¹H. S. Park, D. D. Ryutov, J. S. Ross, N. L. Kugland, S. H. Glenzer, C. Plechaty, S. M. Pollaine, B. A. Remington, A. Spitkovsky, L. Gargate, G. Gregori, A. Bell, C. Murphy, Y. Sakawa, Y. Kuramitsu, T. Morita, H. Takabe, D. H. Froula, G. Fiksel, F. Miniati, M. Koenig, A. Ravasio, A. Pelka, E. Liang, N. Woolsey, C. C. Kuranz, R. P. Drake, and M. J. Grosskopf, *High Energy Density Physics* **8**, 38 (2012).
- ³²Y. Kuramitsu, Y. Sakawa, T. Morita, C. D. Gregory, J. N. Waugh, S. Dono, H. Aoki, H. Tanji, M. Koenig, N. Woolsey, and H. Takabe, *Physical Review Letters* **106**, 175002 (2011).
- ³³T. Morita, Y. Sakawa, Y. Kuramitsu, S. Dono, H. Aoki, H. Tanji, T. N. Kato, Y. T. Li, Y. Zhang, X. Liu, J. Y. Zhong, H. Takabe, and J. Zhang, *Physics of Plasmas* **17**, 122702 (2010).
- ³⁴M. Edamoto, T. Morita, N. Saito, Y. Itadani, S. Miura, S. Fujioka, H. Nakashima, and N. Yamamoto, *Review of Scientific Instruments* **89** (2018).
- ³⁵T. Morita, M. Edamoto, S. Miura, A. Sunahara, N. Saito, Y. Itadani, T. Kojima, Y. Mori, T. Johzaki, Y. Kajimura, S. Fujioka, A. Yogo, H. Nishimura, H. Nakashima, and N. Yamamoto, *Scientific Reports* **7**, 8910 (2017).
- ³⁶J. Sheffield, D. Froula, S. H. Glenzer, N. C. Luhmann, and Jr., *Plasma Scattering of Electromagnetic Radiation: Theory and Measurement Techniques*, (Academic Press Inc 2010).
- ³⁷T. Morita, Y. Sakawa, K. Tomita, T. Ide, Y. Kuramitsu, K. Nishio, K. Nakayama, K. Inoue, T. Moritaka, H. Ide, M. Kuwada, K. Tsubouchi, K. Uchino, and H. Takabe, *Physics of Plasmas* **20**, 092115 (2013).
- ³⁸H.-K. Chung, M. H. Chen, W. L. Morgan, Y. Ralchenko, and R. W. Lee, *High Energy Density Physics* **1**, 3 (2005).
- ³⁹C. K. Li, D. D. Ryutov, S. X. Hu, M. J. Rosenberg, A. B. Zylstra, F. H. Séguin, J. A. Frenje, D. T. Casey, M. Gatun Johnson, M. J.-E. Manuel, H. G. Rinderknecht, R. D. Petrasso, P. A. Amendt, H. S. Park, B. A. Remington, S. C. Wilks, R. Betti, D. H. Froula, J. P. Knauer, D. D. Meyerhofer, R. P. Drake, C. C. Kuranz, R. Young, and M. Koenig, *Physical Review Letters* **111**, 235003 (2013).
- ⁴⁰C. K. Li, P. Tzeferacos, D. Lamb, G. Gregori, P. A. Norreys, M. J. Rosenberg, R. K. Follett, D. H. Froula, M. Koenig, F. H. Séguin, J. A. Frenje, H. G. Rinderknecht, H. Sio, A. B. Zylstra, R. D. Petrasso, P. A. Amendt, H. S. Park, B. A. Remington, D. D. Ryutov, S. C. Wilks, R. Betti, A. Frank, S. X. Hu, T. C. Sangster, P. Hartigan, R. P. Drake, C. C. Kuranz, S. V. Lebedev, and N. C. Woolsey, *Nature Communications* **7**, 1 (2016).
- ⁴¹F. F. Chen, *Introduction to plasma physics and controlled fusion*, 3rd ed. (Springer, 2016).
- ⁴²D. D. Ryutov, R. P. Drake, and B. A. Remington, *The Astrophysical Journal Supplement Series* **127**, 465 (2000).
- ⁴³M. J. Rosenberg, C. K. Li, W. Fox, I. Igumenshchev, F. H. Séguin, R. P. Town, J. A. Frenje, C. Stoeckl, V. Glebov, and R. D. Petrasso, *Nature Communications* **6**, 6190 (2015).
- ⁴⁴G. Fiksel, W. Fox, A. Bhattacharjee, D. H. Barnak, P. Y. Chang, K. Germaschewski, S. X. Hu, and P. M. Nilson, *Physical Review Letters* **113**, 105003 (2014).
- ⁴⁵C. K. Li, F. H. Séguin, J. A. Frenje, J. R. Rygg, R. D. Petrasso, R. P. J. Town, P. A. Amendt, S. P. Hatchett, O. L. Landen, A. J. Mackinnon, P. K. Patel, V. A. Smalyuk, T. C. Sangster, and J. P. Knauer, *Physical Review Letters* **97**, 135003 (2006).